SINTERING SIMULATION OF PIM STAINLESS STEEL

Deborah C. Blaine, Randall M. German

Center for Innovative Sintered Products
The Pennsylvania State University
University Park, Pennsylvania 16802

ABSTRACT

The well-known linear-viscous constitutive model for sintering of a porous body is investigated for specific application to the 17-4 PH stainless steel, injection-molded, hydrogen-sintered system. This model is implemented using Abaqus through the CREEP subroutine. Modification of this model to include a Bingham type yield stress is discussed. Due to the multi-phase characteristic of the 17-4 PH sintering system, this model shows that a simple, single-phase, diffusion-based viscosity does not offer enough complexity to simulate the sintering of this material accurately. This model does simulate a single-phase system like nickel well, which leads to the conclusion that further development of viscosity models could lead to a useful model for multi-phase systems.

INTRODUCTION

Powder injection molding (PIM) entered the powder metallurgy industry with its first patent in 1938. Since then it has evolved into a multimillion-dollar global market. The growth in this field in the last five years has been significant [1]. While Europe and Asia have made a serious commitment to PIM with full-scale production plants, many North American enterprises are still testing the waters, with only a few players going full-scale. As a result of technology development, confidence in this field is picking up. Sales per employee have reached over the $100,000 mark and research into methods for improving productivity and design is becoming more critical.

Computer modeling is a powerful technique for aiding design and improving productivity of engineering processes. For PIM modeling efforts involve the injection molding, debinding, and sintering process. As with any type of modeling, it is vital that the mechanism being described is fully understood for the model to yield meaningful and accurate results. To date, significant effort has been dedicated to the development of models describing sintering kinetics. However, modeling of the sinter process is still too inaccurate to be commercially useful.

There are two basic approaches to the modeling of sintering that have been explored: one is mechanistic, based on modeling the particle-to-particle contacts and contact area growth, merged with models of diffusional flow mechanisms used to describe sintering [3-19]. The other more recent trend uses a continuum model, based on plastic and viscous flow theories, to describe the overall densification of the material [20-36].

In this paper, a continuum model is used, based on the sintering kinetics of a porous linear-viscous material. The effective equivalent stress relates to the effective equivalent strain rate through the material

mechanical response parameters, normalized shear and bulk viscosity. The viscosity parameters are normalized by the material viscosity and dependent on the porosity. It is therefore crucial that a thorough understanding of the viscous response of a material during sintering is acquired.

At present most models describe the behavior of materials during sintering as Newtonian where the strain rate response to stress is linear. In this paper a Bingham response is investigated as a more accurate rheological response model for simulating sintering of injection molded particulate materials. A Bingham response assumes a minimum yield strength has to be reached before material flow occurs [36-37]. The material chosen for this study is injection-molding grade 17-4 PH stainless steel. This material is becoming increasingly popular in the PIM industry due to its high-corrosion resistance qualities and thus makes it apt for demonstration purposes.

EXPERIMENTAL PROCEDURE

Sintering experiments were run on an Anter (Model 1161) vertical pushrod dilatometer to measure the shrinkage behavior during sintering. A sketch showing the dilatometer furnace chamber setup is shown in Figure 1.

The sample used in the experiments was cut from the gate of injection molded tensile bars. The bars were injection molded by Honeywell using their agar-based binder system with 55%vol. solids loading. The powder used was ATMIX water-atomized 17-4 PH injection-molding grade stainless steel. The powder characteristics are given in Table 1.

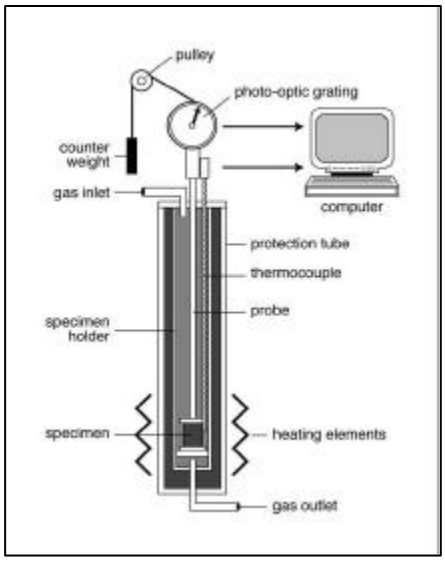

Figure 1. Sketch of dilatometer

Table 1. Powder Characteristics

Particle size:			
D_{10}	**D_{50}**	**D_{90}**	**Mean**
3 μm	5 μm	10 μm	9 μm
Powder density:			
Apparent	**Tap**	**Pycnometer**	
2.85 g/cm^3	4.25 g/cm^3	7.66 g/cm^3	

Thermal debinding was performed in hydrogen after the sample was cut using the following cycle:
room temperature → 2°C/min to 60°C, hold 2hrs → 2°C/min to 110°C, hold1 hr → 2°C/min to 450°C, hold 2hrs → cool at 5°C/min to room temperature.

The sample was then sintered in hydrogen using the following sinter cycle:
room temperature → 10°C/min to 1010°C, hold 1hr → 1.67°C/min to 1365°C, hold 1hr → cool at 10°C/min to room temperature.

The dimensions of the green and debound sample are given in Table 2.

Table 2. Sample #103-15 green and debound dimensions

	Green dimensions	**Debound dimensions**
Top diameter	6.67 mm	6.69 mm
Bottom diameter	7.23 mm	7.23 mm
Height	11.67 mm	11.68 mm
Mass	2.0460 g	2.0044 g
Density	4.6214 g/cc	4.5106 g/cc

CONSTITUTIVE MODEL

The rheological constitutive equation describing the response of linear-viscous porous materials, written in terms of the stress tensor σ_{ij} and the strain rate tensor $\dot{\varepsilon}_{ij}$, is [27]

$$\sigma_{ij} = \frac{\sigma(W)}{W}\left[\varphi\dot{\varepsilon}'_{ij} + \psi\dot{\varepsilon}_{ii}\delta_{ij}\right] + P_L\delta_{ij} \tag{1}$$

where $\sigma(W)$ is the effective equivalent stress, W is the effective equivalent strain rate, $\dot{\varepsilon}'_{ij} = \dot{\varepsilon}_{ij} - \frac{1}{3}\dot{\varepsilon}_{ii}\delta_{ij}$ is the deviatoric strain rate, and P_L is the Laplace stress (sintering stress).

The Laplace stress, in this case defined as the collective action of capillary stresses in a porous material [27], is similar to the bulk sintering stress [37], an equivalent stress distributing the localized capillary stresses at the particle-to-particle contacts out over the compact cross section.

The effective equivalent stress $\sigma(W)$ determines the rheological response of the material through its relation with the effective equivalent strain W, defined as

$$W = \sqrt{\frac{\varphi\dot{\gamma}_e^2 + \psi\dot{\varepsilon}_{ii}^2}{1-\theta}} \tag{2}$$

where θ is the porosity, and $\dot{\gamma}_e$ is the equivalent shear strain rate.

$$\dot{\gamma}_e = \sqrt{\dot{\varepsilon}'_{ij}\dot{\varepsilon}'_{ij}} \tag{3}$$

For a porous body the rheological response described by $\sigma(W)$ is limited on one side by rigid-plastic response, $\sigma(W) = \tau_o$ and on the other by the linear-viscous case, $\sigma(W) = 2\eta W$. The rigid-plastic response assumes that body fully yields once τ_o, the yield stress for the fully dense material is reached. The linear-viscous (Newtonian) case assumes that $\sigma(W)$ is linearly related to W by the apparent viscosity η, equivalent to the shear viscosity for the fully dense material.

The Bingham response lies somewhere between the linear-viscous and rigid-plastic response: the material does not deform until a yield stress is reached, and beyond that point it experiences linear-viscous flow, $\sigma(W) = 2\eta W - \tau_o$. The intercept is chosen as a negative value as the flow that correlates to shrinkage is due to an effective compressive (-ive) sinter stress. Each rheological response is shown graphically in Figure. 2.

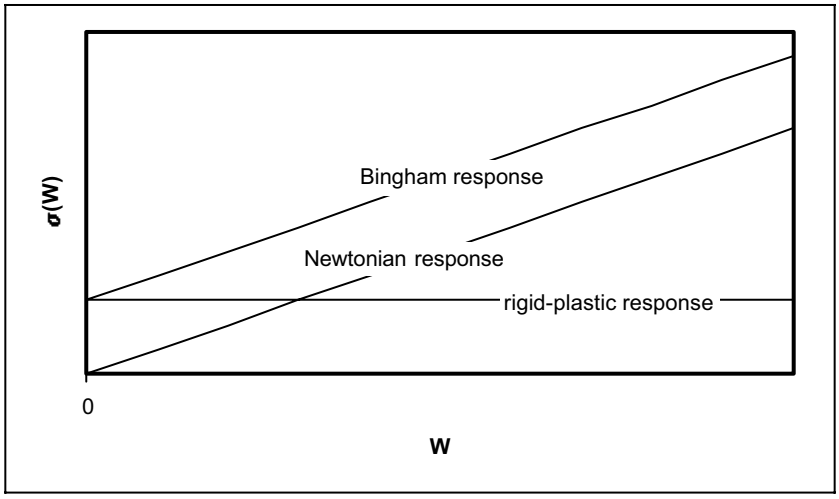

Figure 2. Rheological responses of materials

The temperature dependent apparent viscosity can be determined from the diffusivity of the material

$$\eta = \frac{r_o}{D} = \frac{r_o^3 kT}{[\delta D_b + r_o(\theta_o - \theta)D_v]\Omega} \tag{4}$$

where r_o is the initial particle radius, k is Boltzmann's constant, T is temperature, δD_b is the product of the grain boundary width and the grain boundary diffusivity, θ is the porosity and the subscript o represents the initial porosity, D_v is the volume diffusivity, and Ω is the atomic volume. The grain boundary diffusivity has an Arrenhius type dependence

$$\delta D_b = (\delta D_b)_o e^{Q_b/RT} \tag{5}$$

where $(\delta D_b)_o$ is the pre-exponent for grain boundary diffusion, Q_b is the activation energy for grain boundary diffusion, R is the universal gas constant, and T is the temperature. This Arrenhius type dependence applies to the volume diffusivity too

$$D_v = (D_v)_o e^{Q_v/RT} \tag{6}$$

where (D_v) is the pre-exponent for volume diffusion, Q_v is the activation energy for volume diffusion, and R and T are the same as in equation (5). Typical values for the diffusion parameters as well as the activation energies are given in Table 3. The values given are for 316L stainless steel, and pure iron.

Table 3. Diffusivity pre-exponents and activation energies

	$D_{v,}$ m^3/s	$Q_{v,}$ kJ/mol	$\delta D_{b,}$ m^2/s	$Q_{b,}$ kJ/mol
Iron	2x10-4	239	1.10e-17	128
316L stainless	4x10-5	280	2x10-13	167

There is no available information for 17-4PH stainless steel, but even if there were it should be noted that these values vary orders of magnitude between sources making it extremely difficult to find an accurate value for viscosity[42].

The equation for the apparent viscosity can therefore be simplified to an Arrenhius type equation, with all the influencing parameters collected into an experimentally determinable viscosity pre-exponent η_o and an activation energy for viscous flow Q.

$$\eta = \eta_o e^{Q/RT} \tag{7}$$

Applying the Bingham response to equation (1) gives the following

$$\sigma_{ij} = \frac{2\eta W - \tau_0}{W}\left[\varphi \varepsilon'_{ij} + \psi \varepsilon_{ii}\delta_{ij}\right] + P_L\delta_{ij} \approx 2\eta\left[\varphi \varepsilon'_{ij} + \psi \varepsilon_{ii}\delta_{ij}\right] + (P_L - \tau_0)\delta_{ij} \tag{8}$$

The stress invariants can be calculated from this equation: the effective shear stress is

$$\tau = \sqrt{\sigma'_{ij}\sigma'_{ij}} = 2\eta\varphi\gamma \tag{9}$$

and the hydrostatic pressure is

$$p = \frac{\sigma_{ii}}{3} = 2\eta\psi\dot{\varepsilon}_{ii} + P_L - \tau_0 \tag{10}$$

where $\dot{\varepsilon}_{ii}$ is the volumetric shrinkage rate.

An important relationship, true for any rheological response $\sigma(W)$, between these stress invariants is determined from equation (9) and (10)

$$\tau\psi\dot{\varepsilon}_{ii} = (p - P_L)\varphi\gamma \tag{11}$$

The normalized shear and bulk viscosities are defined by[27]

$$\varphi = \frac{G}{\eta} = (1-\theta)^2 \tag{12}$$

$$\psi = \frac{K}{2\eta} = \frac{2}{3}\frac{(1-\theta)^3}{\theta} \tag{13}$$

where G and K are the shear and bulk moduli respectively.

The sintering stress has been related to porosity by many models [27]. In this case we use the following definition

$$P_L = \frac{3\alpha}{r_o}(1-\theta)^2 \tag{14}$$

where α is the surface energy and r_o is the initial particle radius.

FINITE ELEMENT MODELING

For FEM analysis, the Abaqus CREEP subroutine is used to model the sintering behavior [41]. The rate dependent plasticity equation describing material response in the CREEP subroutine is

$$\dot{\varepsilon}_{ij}^{pl} = \bar{\dot{\varepsilon}}^{cr}\underline{n} + \frac{1}{3}\bar{\dot{\varepsilon}}^{sw}\underline{I} \tag{15}$$

where $\bar{\dot{\varepsilon}}^{cr}$ is the equivalent creep strain rate (a scalar quantity), $\bar{\dot{\varepsilon}}^{sw}$ is the equivalent swelling strain rate (a scalar quantity), $\underline{n}$ is the gradient of the deviatoric stress potential and $\underline{I}$ is the unit matrix (equivalent to δ_{ij}).

The constitutive law for sintering given by equation (8) has to be arranged in the same form as equation (15) for implementation in Abaqus. The stress tensor decomposition is given by

$$\sigma_{ij} = \sigma'_{ij} + p\delta_{ij} \tag{16}$$

and strain rate decomposition by

$$\dot{\varepsilon}_{ij} = \dot{\varepsilon}'_{ij} + \frac{\dot{\varepsilon}_{ii}}{3}\delta_{ij} \tag{17}$$

Applying equations (16) and (17) to equation (8) gives the Bingham response constitutive equation rearranged with the strain rate as the independent variable for $P_L > \tau_o$

$$\dot{\varepsilon}_{ij} = \frac{1}{2\eta}\left[\frac{\sigma'_{ij}}{\varphi} + \frac{p - (P_L - \tau_0)}{3\psi}\delta_{ij}\right] \tag{18}$$

Comparing equation (18) to equation (15) gives the following relationship for the equivalent swelling strain rate

$$\bar{\dot{\varepsilon}}^{sw} = \frac{1}{2\eta}\left[\frac{p - (P_L - \tau_0)}{\psi}\right]\delta_{ij} \tag{19}$$

Note that the hydrostatic pressure p in this paper is defined by equation (10), however in Abaqus it has the opposite sign (-).

To find the similar relationship for equivalent creep strain rate consider the definition of the Mises or equivalent stress given in Abaqus

$$q = \sqrt{\frac{3}{2}\sigma'_{ij}\sigma'_{ij}} = \sqrt{\frac{3}{2}\left[\sigma_{ij}\sigma_{ij} - \frac{1}{3}\sigma_{kk}^2\right]} \tag{20}$$

The gradient of the deviatoric stress potential is defined by

$$n_{ij} = \frac{\partial q}{\partial \sigma_{ij}} = \frac{3}{2q}\sigma'_{ij} \tag{21}$$

Now substituting equation (21) into equation (15),

$$\dot{\varepsilon}'_{ij} = \bar{\dot{\varepsilon}}^{cr} n_{ij} = \bar{\dot{\varepsilon}}^{cr}\frac{3}{2q}\sigma'_{ij} \tag{22}$$

and comparing equation (22) to equation (18), determine the expression for the equivalent creep strain rate

$$\bar{\dot{\varepsilon}}^{cr} = \frac{1}{2\eta\varphi}\frac{2q}{3} = \frac{q}{3\eta\varphi} \tag{23}$$

Using equations (19) and (23) along with equations (12), (13) and (14) the sintering behavior can be modeled using Abaqus.

As we are dealing with the case of free sintering, $p = 0$, and the equation (18) reduces to

$$\varepsilon_{ij} = \frac{1}{2\eta}\left[\frac{\sigma'_{ij}}{\varphi} - \frac{(P_L - \tau_0)}{3\psi}\delta_{ij}\right] \tag{24}$$

For further simplification, the influence of deviatoric stresses, such as gravity, internal residual stresses or dilatometer pushrod force, are ignored, and isotropic shrinkage is assumed. This leads to a direct relationship between volumetric shrinkage, sintering stress and threshold stress:

$$\varepsilon_{ii} = -\frac{(P_L - \tau_0)}{6\eta\psi} \tag{25}$$

From equation (25) it is clear that the compact shrinks in linear relation with the sintering stress, related through the viscosity and to the porosity, once a threshold stress has been reached. It is important to note that this Bingham response equation hold true only for $P_L > \tau_o$. For $P_L < \tau_o$ there is no shrinkage.

RESULTS AND DISCUSSION

For the purposes of this study a comparison of results obtained using a constant threshold strength of 1Mpa, which is in the same range as the sintering stress [37], is used throughout the sinter cycle.

Using the diffusivity data in Table 3. along with equation (7) to calculate the viscosity in the simulation proved ineffective. The shrinkage obtained was orders of magnitude too small. By fitting a curve to the diffusivity-based viscosity of the form of equation (8) , and scaling the viscosity down until the simulation results were in the same range as the dilatometer results, satisfactory results were obtained as shown in Figure 3 .

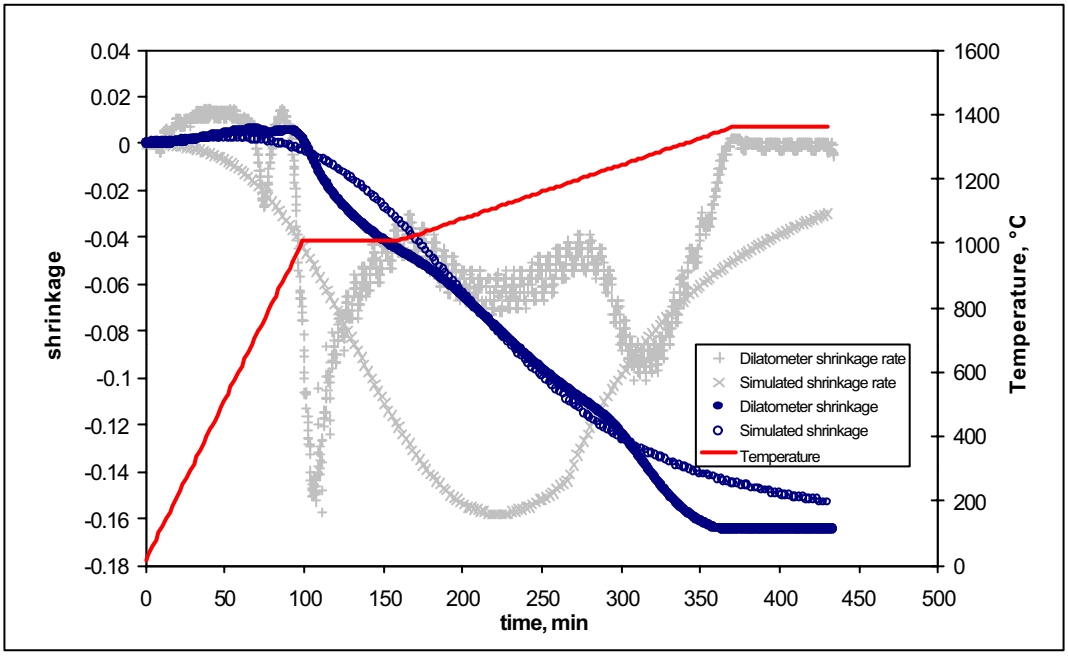

Figure 3. Simulated shrinkage compared to experimental dilatometer shrinkage for 17-4 PH. Shrinkage rate and temperature profile are also shown.

The simulated results show the thermal expansion that occurs to just before 1000°C, at which point shrinkage starts. For the simulated results, the shrinkage shows a smooth curve, which does not mimic the experimental results. The reason for this is the choice of one viscosity relationship for the entire sinter cycle,

$$\eta = \eta_o e^{Q/RT} = 3.4 \cdot 10^7 e^{27,500/RT} \quad (25)$$

In the case of a single-phase solid state sintering system, such as with nickel, the use of one viscosity equation for the whole sinter cycle is warranted. The viscosity is linked to the diffusion parameters of nickel, and these parameters do not change during sintering for a single-phase system. The simulation yields good results as is shown in Figure 4. where nickel dilatometry has been simulated.

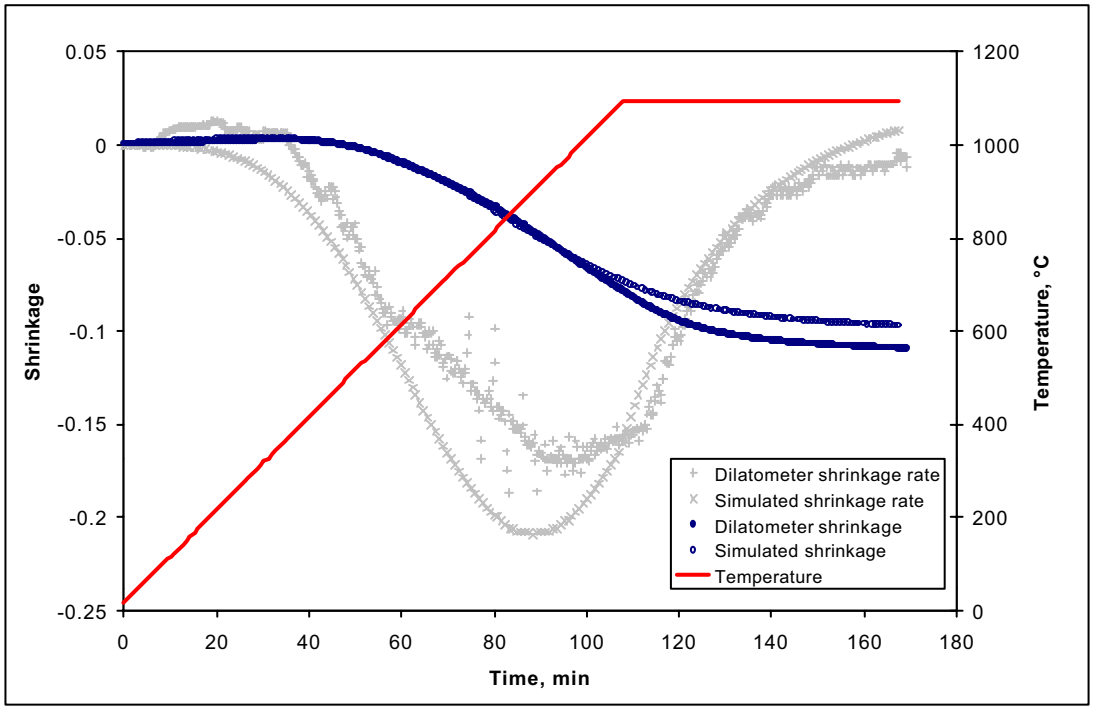

Figure 3. Simulated shrinkage compared to experimental dilatometer shrinkage for Nickel. Shrinkage rate and temperature profile is also shown.

In the case of 17-4 PH there are a couple of phase transformations that the material goes through during sintering [43]. Due to these phase transformations the shrinkage is not as smooth and continuous as for the single-phase system of nickel.

First of all, for 17-4 PH, around 780°C there is a phase transformation from the room temperature martensitic phase to austenite. As martensite has a BCT (body-centered tetragonal) atomic structure, and austenite has a FCC (face-centered cubic) atomic structure that occupies less volume than the BCT

structure, this phase transformation is associated with volumetric shrinkage. The simulation does not mimic this phase transformation, as the only factors affecting expansion (or shrinkage) in the model are thermal expansion and viscosity.

At around 1220°C, there is prominent delta-ferrite formation along the grain boundaries and at the pores. Delta ferrite has a BCC (body-centered cubic) atomic structure, which like BCT is more loosely packed than the FCC austenitic structure. This looser structure allows diffusion to occur more easily, in other words, the diffusion parameters for the austenitic phase are different for those of the ferritic phase in 17-4 PH. Thus the viscosity drops and shrinkage rate increases. This can be clearly seen by comparing the simulated and dilatometer shrinkage in Figure 3. At 1220°C the significant change in the shrinkage rate causes the compact to densify to its maximum value before it even reaches the last hold temperature at 1365°C. Seeing as the simulation uses only one equation for viscosity, based on 316L stainless steel that is austenitic, once the atomic diffusion becomes dominated by the delta ferrite phase, the viscosity value is too high and the associated shrinkage rate is too slow. The resultant simulated shrinkage is too small.

CONCLUSIONS

While this model offers a good correlation for a single-phase system, the results for a multi-phase, and conceivably for a liquid-phase system, are not accurate. Further development of a viscosity model is needed to control the shrinkage rate through implementation in the constitutive model. Also while the general form of a diffusion-based viscosity allows for an accurate representation of shrinkage during sintering, the viscosity has to be scaled several orders of magnitude before an accurate result is found. This again leads to the conclusion that further investigation into what influences viscosity, and how to estimate in-situ viscosity for a sinter compact is needed.
Development of this model needs to incorporate a more in-depth study of the exact interaction between the capillary strength and the yield strength, and their evolution with during the sinter cycle.

REFERENCES

[1] R.M. German, and R. Cornwall, *Powder Injection Molding – An industry and market report,* Innovative Material Solutions, Inc., State College, PA, 2000.
[2] R.M. German, *Sintering Theory and Practice,* Wiley-Interscience, New York, NY, 1996.
[3] G.C. Kuczynski, *Trans. AIME,* 1949, vol. 185, pp.169-
[4] R.L. Coble, "Sintering Crystalline Solids I. Intermediate and Final State Diffusion Models", *J. Applied Physics,* Vol. 32, No. 5, 1961, pp.784-792
[5] D. Lynn Johnson, "A General Model for the Intremediate Stage of Sintering", *J. Am. Ceram. Soc.,* Vol. 53, No. 10, 1970, pp. 574-577
[6] A.J. Markworth, "On Volume-diffusion-controlled Final-stage Densification of a Porous Solid", *Scripta Metall.,* Vol. 6, 1972, pp. 957-960
[7] M.F. Ashby, "A First Report on Sintering Diagrams", *Acta Metall.,* Vol. 22, 1974, pp. 275-285
[8] F.B. Swinkels, and M.F. Ashby, "A Second Report on Sintering Diagrams", *Acta Metall.,* Vol. 29, 1981, pp.259-281
[9] K.-S. Hwang, R.M. German, and F.V. Lenel, "Analysis of Initial Stage Sintering Through Computer Simulation", *Powder Metall. Int.,* Vol. 23, No. 2, 1991, pp. 86-91
[10] J.D. Hansen, R.P. Rusin, M.-H. Teng, and D. Lynn Johnson, 'Combined-Stage Sintering Model", *J. Am. Ceram. Soc.,* Vol. 75, No. 5, 1992, pp. 1129-1135
[11] D. Lynn Johnson, *Mater. Sci. Monographs,* 1981, vol.14, pp. 17-26

[12] J.L. Johnson, and R.M. German, "Solid-State Contributions to Densification During Liquid-Phase Sintering", *Metall. Mater. Trans. B,* vol. 27B, 1996, pp. 901-909
[13] R.M. German, "Supersolidus Liquid-phase Sintering of Prealloyed Powders", *Metall. Mater. Trans. A,* vol. 28A, 1997, pp. 1553-1567
[14] J.L. Shi, "Solid State Sintering of Ceramics: Pore microstructure Models, Densification Equations and Applications", *J. Mater. Sci.*, vol. 34, 1999, pp. 3801-3812
[15] R.M. McMeeking, and L.T. Kuhn, "A Diffusional Creep Law for Powder Compacts", *Acta Metall. Mater.,* Vol. 40, No. 5, 1992, pp. 961-969
[16] J. Svoboda, and H. Riedel, "Quasi-equilibrium Sintering for Coupled Grain-boundary and Surface Diffusion", *Acta Metall. Mater.,* Vol. 43, No. 2, 1995, pp.499-506
[17] J. Svoboda, and H. Riedel, "New Solutions Describing the Formation of Inetrparticle Necks in Solid-state Sintering", *Acta Metall. Mater.,* Vol. 43, No. 1, 1995, pp.1-10
[18] H. Riedel, V. Kozák, and J. Svoboda, "Densification and Creep in Final Stage of Sintering", *Acta Metall. Mater.,* Vol. 42, No. 9, 1994, pp.3093-3103
[19] H. Riedel, and J. Svoboda, "A Theoretical Study of Grain Growth in Porous Solids During Sintering", *Acta Metall. Mater.,* Vol. 41, No. 6, 1993, pp. 1929-1936
[20] V.V. Skorohod, E.A. Olevsky, and M.B. Shtern, 'Continuum Theory for Sintering of the Porous Bodies: Model and Application", *Sci. Sinter.,* Vol. 23, No. 2, 1991, pp. 79-91
[21] H. Riedel, D. Meyer, J. Svoboda, and H. Zipse, "Numerical Simulation of Die Pressing and Sintering - Development of Constitutive Equations", *Int. J. Met. & Hard Mater.,* Vol. 12, 1993-4, pp.55-60
[22] H. Zipse, "Finite-Element Simulation of the Die Pressing and Sintering of a Ceramic Component", *J. Europ. Ceram. Soc.,* Vol. 17, 1997, pp.1707-1713
[23] A.C.F. Cocks, "The Structure of Consitutive Laws for the Sintering of Fine Grained Materials" *Acta Metall. Mater.,* Vol. 42, No. 7, 1994, pp. 2191-2210
[24] Z.-Z. Du, and A.C.F. Cocks, "Constitutive Models for the Sintering of Ceramic Components - I. Material Models", *Acta Metall. Mater.,* Vol. 40, No. 8, 1992, pp.1969-1979
[25] Z.-Z. Du, and A.C.F. Cocks, "Constitutive Models for the Sintering of Ceramic Components - II. Sintering of Inhomogeneous Bodies", *Acta Metall. Mater.,* Vol. 40, No. 8, 1992, pp.1981-1994
[26] J. Besson, and M. Abouaf, "Grain Growth Enhancement in Alumina during Hot Isostatic Pressing", *Acta Metall. Mater.,* Vol. 39, No. 10, 1991, pp.2225-2234
[27] E.A. Olevsky, "Theory of Sintering: from discrete to continuum", *Mater. Sci. & Eng. R,* Vol. 23R, 1998, pp.41-100
[28] E.A. Olevsky, and R.M. German, "Effect of Gravity on Dimensional Change During Sintering - I. Shrinkage Anisotropy", *Acta Mater.,* Vol. 48, 2000, pp.1153-1166
[29] M. Gasik, and B. Zhang, "A Constitutive Model and FE simulation for the Sintering Process of Powder Compacts", *Comp. Mater. Sci.,* Vol. 18, 2000, pp. 93-101
[30] K.T. Kim, and Y.C. Jeon, "Densification Behaviour of 316L Stainless Steel Powder Under High Temperature", *Mater. Sci. & Eng. A,* Vol. A245, 1998, pp. 64-71
[31] J. Svoboda, H. Riedel, and H. Zipse, "Equilibrium Pore Surfaces, Sintering Stresses and Constitutive Equations for Intermediate and Late Stages of Sintering - I. Computation of Equilibrium Surfaces", *Acta Metall. Mater.,* Vol. 42, No. 2, 1994, pp.435-443
[32] J. Svoboda, H. Riedel, and H. Zipse, "Equilibrium Pore Surfaces, Sintering Stresses and Constitutive Equations for Intermediate and Late Stages of Sintering - II. Diffusional Densification and Creep", *Acta Metall. Mater.,* Vol. 42, No. 2, 1994, pp.445-452
[33] O. Gillia, and D. Bouvard, "Phenomenological Analysis of Densification Kinetics During Sintering: Application to WC-Co Mixture", *Mater. Sci. & Eng. A,* Vol. A279, 2000, pp.185-191
[34] R.K. Bordia, and G.W. Scherer, "Overview No. 70: On Constrained Sintering - I Consitutive Model for a Sintering Body", *Acta Metall.,* Vol. 36, No. 9, 1988, pp.2393-2397
[35] R.K. Bordia, and G.W. Scherer, "Overview No. 70: On Constrained Sintering - II Comparison of Constitutive Models", *Acta Metall.,* Vol. 36, No. 9, 1988, pp.2399-2409

[36] E.A. Olevsky, G.A. Shoales, and R.M. German, "Temperature Effect on Strength Evolution Under Sintering", *Mater. Res. Bull.,* Vol. 36, 2001, pp.449-459
[37] R.M. German, "Manipulation of Strength During Sintering as a Basis for Obtaining Rapid Densification without Distortion", *Mater. Trans.,* Vol. 42, No. 7, 2001, pp.1400-1410
[38] G.A. Shoales, and R.M. German, 'Combined Effects of Time and Temperature on Strength Evolution Using Integral Work-of-Sintering Concepts", *Metall. Mater. Trans. A,* Vol. 30A, 1999, pp.465-470
[39] O. Gillia, C. Josserond, and D. Bouvard, "Viscosity of WC-Co Compacts during Sintering", *Acta Mater.,* Vol. 49, 2000, pp.1413-1420
[40] D. Bouvard, and T. Meister, "Viscosity of WC-Co Compacts during Sintering", *Model. Simul. Mater. Sci. Eng.,* Vol. 8, 2000, pp.377-388
[41] Abaqus Theory Manual versions 5.8, 1998
[42] I. Kaur, W. Gust, and L. Kozma, *Handbook of Interphase Boundary Diffusion Data,* 1989, Ziegler Press, Stuttgart
[43] Y. Wu, D. Blaine, B. Marx, C. Schlaefer, and R. German, "Sintering Densification and Microstructure Evolution of Injection-Molding Grade 17-4 PH Stainless Steel Powder", *Mat. and Metal. Trans. A,* Vol. 33A, 2002, press